Precision Agriculture (2021) 22:1263–1283
https://doi.org/10.1007/s11119-020-09783-7

# Upscaling proximal sensor N-uptake predictions in winter wheat (*Triticum aestivum* L.) with Sentinel-2 satellite data for use in a decision support system

**S. Wolters[1] · M. Söderström[1] · K. Piikki[1] · H. Reese[2] · M. Stenberg[3]**

Accepted: 30 December 2020 / Published online: 21 January 2021


## Abstract

Total nitrogen (N) content in aboveground biomass (N-uptake) in winter wheat (*Triticum aestivum* L.) as measured in a national monitoring programme was scaled up to full spatial coverage using Sentinel-2 satellite data and implemented in a decision support system (DSS) for precision agriculture. Weekly field measurements of N-uptake had been carried out using a proximal canopy reflectance sensor (handheld Yara N-Sensor) during 2017 and 2018. Sentinel-2 satellite data from two processing levels (top-of-atmosphere reflectance, L1C, and bottom-of-atmosphere reflectance, L2A) were extracted and related to the proximal sensor data (n = 251). The utility of five vegetation indices for estimation of N-uptake was compared. A linear model based on the red-edge chlorophyll index (CI) provided the best N-uptake prediction (L1C data: $r^2 = 0.74$, mean absolute error; MAE = 14 kg ha$^{-1}$) when models were applied on independent sites and dates. Use of L2A data, rather than L1C, did not improve the prediction models. The CI-based prediction model was applied on all fields in an area with intensive winter wheat production. Statistics on N-uptake at the end of the stem elongation growth stage were calculated for 4169 winter wheat fields > 5 ha. Within-field variation in predicted N-uptake was > 30 kg N ha$^{-1}$ in 62% of these fields. Predicted N-uptake was compared against N-uptake maps derived from tractor-borne Yara N-Sensor measurements in 13 fields (1.7–30 ha in size). The model based on satellite data generated similar information as the tractor-borne sensing data ($r^2 = 0.81$; MAE = 7 kg ha$^{-1}$), and can therefore be valuable in a DSS for variable-rate N application.

**Keywords** Decision support system · L2A · Nitrogen fertilisation · Precision agriculture · Sentinel-2 · Variable rate application

✉ S. Wolters
sandra.wolters@slu.se

[1] Department of Soil & Environment, Swedish University of Agricultural Sciences (SLU), Skara, Sweden

[2] Department of Earth Sciences, University of Gothenburg, Gothenburg, Sweden

[3] Swedish Board of Agriculture, Skara, Sweden

## Introduction

Winter wheat (*Triticum aestivum* L.) is an important crop globally, and is often the main crop in northern European cropping schemes. Much of the arable land in Sweden is dedicated to winter wheat production (19% of total cropping area and 48% of total grain production) (Swedish Board of Agriculture 2019a). Fertilisation with nitrogen (N) is often performed in two or three steps between the developmental stages of tillering and booting, to match crop requirements. Making decisions on the frequency, timing and quantity of this supplementary fertilisation can be a challenge for farmers, who try to find an economically optimum level in fertilisation. The estimation of the N concentration in aboveground plant tissues multiplied by above-ground dry matter mass (here denominated as N-uptake) during the period of supplementary fertilisation is an important component in the formulation of a fertilisation strategy (Schils et al. 2018). There are both economic and environmental benefits in optimising N fertilisation, since it optimises the quantity and quality of the crop in relation to the production costs and at the same time helps prevent losses of excess N through leaching or denitrification (e.g. Delin and Stenberg 2014; Swedish Board of Agriculture 2019a). Optimisation can be done on different scales, by fertilising different fields in different ways or by fertilising individual fields using a variable rate (variable rate application, VRA). It is known that growing conditions are often non-uniform between and within cropping fields (e.g. Sawyer 1994; Stafford 2000). Thus VRA of N fertiliser based on estimated N-uptake at the time of fertilisation is likely to better meet crop demands than uniform application. Variable application of N fertiliser can also be carried out for the purpose of reaching target levels of grain protein content, which is an important quality aspect (Basnet et al. 2003; Börjesson et al. 2019; Söderström et al. 2010).

Estimation of N-uptake in winter wheat can be done in multiple ways. Optical remote sensing is a method that has gained interest in recent decades, due to relatively easy and affordable application in the field (Berger et al. 2020; Mulla 2013; Zhao 2005). The N-status of crops can be estimated with optical sensing instruments by estimation of leaf chlorophyll concentration and biomass volume (Curran 1989; Kokaly 2001). Optical sensors measure canopy reflectance in different regions of the electromagnetic spectrum. Proximal crop canopy optical sensors have been available to farmers and advisors for many years (Reusch 2003; Singh 2019). These can be mounted on a vehicle, such as a tractor, or can be used as a handheld instrument. Limitations of this approach are that users rely on costly equipment and that collection of sensor data in the field can be time-consuming, making this method less feasible or attractive for some farmers.

The Swedish Board of Agriculture (Jordbruksverket, Jönköping, Sweden) provides weekly assessments to farmers on N-uptake in winter wheat based on measurements using the handheld version of the Yara N-Sensor® (Yara Gmbh, Hanninghof, Germany; as described by Reusch 2005). The measurements are taken at about 40 point locations in each year across the major agricultural regions in Sweden. They have been carried out to create up-to-date advice for farmers and advisors based on N-uptake measurements in unfertilised plots (N-uptake in unfertilised plots, so called zero-plots, is an indication of soil N-supply) during the period of supplementary fertilisation. Measurements were also made in an area of the field judged to be uniform and with no experimental manipulation (i.e. managed by the farmer as usual). The results are reported to farmers and advisors through an internet service (www.greppa.nu). This campaign generated a continuous time series of N-uptake, as measured by the N-sensor, but with no spatial coverage.

A development could be to scale this point information using satellite remote sensing to full spatial coverage using optical satellite imagery. The Copernicus Sentinel-2 mission comprises a constellation of two polar-orbiting satellites (2A, 2B) placed in a sun-synchronous orbit, and phased 180° to each other (Fletcher 2012, Drusch 2012). The instrument has a swath width of 290 km and a revisit time of 5 days at the equator. At Swedish latitudes, the temporal frequency for obtaining a new satellite product is every 2–3 days. This temporal frequency may be sufficient for practical use in time-critical, within-season N-status monitoring in grain crops.

Sentinel-2 data are published in different levels of processing, as top-of-atmosphere (TOA) data (L1C) and bottom-of-atmosphere (BOA) data (L2A) (ESA 2020). L1C products have been disseminated by ESA since June 2015 and L2A products from May 2017. The L1C products are $100 \times 100$ km$^2$ tiles with radiometric and geometric corrections, including orthorectification and spatial registration (ESA 2020). L2A products are considered 'analysis-ready products' that should be ready for immediate analysis without the need for further processing, and thereby better estimate reflectance. The L2A correction algorithms used by ESA are based on a series of threshold tests that use as input TOA reflectance from various Sentinel-2 spectral bands and auxillary data, look-up tables derived from a radiative transfer model library and digital elevation model (DEM) data. The processing procedure encompasses six steps: (1) a scene classification procedure to identify clouds, their shadows and snow; (2) aerosol optical thickness (AOT) calculation using a dense dark vegetation algorithm; (3) usage of a differential absorption algorithm to retrieve water vapour (WV); (4) cirrus cloud correction; (5) surface reflectance retrieval; and (6) scene classification with a terrain correction using DEM data. Apart from the corrected result, outputs are an AOT map, a WV map and a scene classification map, together with quality indicators for cloud and snow probabilities (Gascon et al. 2017; Main-Knorn et al. 2017; Mueller-Wilm 2016).

To derive information on crop canopy health and vigour from multispectral satellite data and proximal crop sensors, vegetation indices are often used. Commonly used vegetation indices use bands in the near-infrared (NIR), red and red-edge regions of the electromagnetic spectrum. Red-edge indices in particular have been proposed for intensive crop management applications throughout the growing season (Gitelson et al. 2003; Reusch 2003, 2005; Söderström et al. 2017). Some red- and NIR- based indices lose sensitivity after reaching a threshold level of leaf coverage and/or chlorophyll content, whereas red-edge-based indices are still sensitive to variation in denser canopies (Barnes et al. 2000; Qi et al. 1994; Rouse et al. 1974). The short-wave infrared (SWIR) region has also been shown to be useful in assessment of N content in crops (e.g. Herrmann et al. 2010; Söderström et al. 2010), but many of the crop sensors currently in use lack bands in this region of the electromagnetic spectrum. With hyperspectral and multispectral sensor data, a limitation of the conventional vegetation indices is that only a limited portion of the available data is used. An alternative approach to indices is to apply more advanced multivariate or machine-learning methods to include all bands or, preferably, all relevant bands (Berger et al. 2020; Verrelst et al. 2015). Regardless of the approach used, it is important to properly validate the prediction models, and to make sure there is no overfitting. This is important for model deployment in a decision support system (DSS) for precision agriculture.

Crop canopy N-status information, in the form of vegetation index maps from satellite data, are already available to end-users (e.g. farmers and advisors) via an internet based DSS, such as CropSAT (www.cropsat.com) (Söderström et al. 2017). A DSS can function as a tool to translate reflectance based N-uptake data to N-rate maps (i.e. prescription maps) to be used for VRA of N fertilisers. Agricultural practitioners can

use a DSS to get instant access to inexpensive, yet timely and site-specific, decision support for precision N fertilisation.

Wolters et al. (2019) developed a prediction model based on Sentinel-2 L1C data for generation of N-uptake maps to be used in a DSS. That study demonstrated that a Sentinel-2 L1C-based model could be used to predict N-uptake with different vegetation indices for use in practical applications.

The aim in the present study was to test whether it is possible to scale up the weekly point measurements of the Yara N-Sensor to full spatial coverage of the arable land in southern Sweden, and make the result available in a DSS. Specific objectives were to:

- Develop N-uptake scaling models through scaling handheld proximal sensor data using Sentinel-2 data, and evaluate their performance at independent sites and dates;
- Evaluate differences in model performance between Sentinel-2 processing levels (L1C and L2A) and different vegetation indices;
- Quantify the spatial variation in N-uptake within and between fields, by applying the model in an area in Sweden with intensive winter wheat production; and
- Apply the best scaling model and evaluate the resulting satellite-based N-uptake maps by comparison with N-uptake maps from a commonly used tractor-borne sensor system.

The hypotheses are as follows:

- Handheld N-sensor measurements in winter wheat can be scaled up for use in a DSS for VRA of N.
- The scaled model performs better when based on Sentinel-2 L2A data than when based on L1C data.
- The scaled model produces N-uptake maps that are similar to maps from tractor-borne proximal reflectance sensors.

## Materials and methods

### Study area

The entire study area encompassed a large part of southern Sweden, from roughly 55° to 61° N and from 10° to 19° E (Fig. 1). The temperate climate makes this a suitable area for rain-fed grain production, e.g. the median winter wheat yield during 2015–2019 was 7400 kg $ha^{-1}$ (Statistics Sweden, Örebro, Sweden; www.scb.se). Mean annual precipitation is around 700–1000 mm in the agricultural regions studied, with higher values in western parts, and mean annual temperature is 5–8 °C (Swedish Meteorological and Hydrological Institute, Norrköping, Sweden; www.smhi.se). The cropland (around $2 \times 10^6$ ha) in the region is mainly found on young lacustrine and marine sediments deposited after the Weichselian glaciation (Fredén 1994), with heavy clays in the northeast and mostly loam and sandy loam in the southwest (Piikki and Söderström 2019).

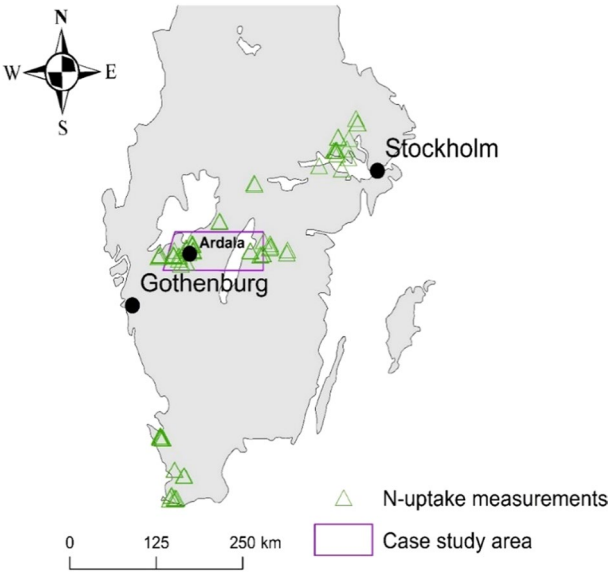


**Fig. 1** The study area including the locations of proximal field data nitrogen (N)-uptake measurements in southern Sweden in winter wheat (*Triticum aestivum* L.). The area northeast of Gothenburg depicts the case study area in which the within-field variability of N-uptake was statistically assessed by deploying the satellite-based prediction model for all winter wheat fields. In the vicinity of the Ardala village, 13 winter wheat fields were scanned with a tractor-borne N-sensor for comparison with the Sentinel-2 based model

## Handheld proximal sensing

The handheld version of the Yara N-Sensor was used by the Swedish Board of Agriculture to collect field data from 40 to 50 farms per year on N-uptake in winter wheat during growth stages DC22-53 (Zadok et al. 1974), in measurements conducted on a weekly basis from late April to early June 2017–2018. In this study, data was used from sensor measurements made in a uniform area of the winter wheat fields, in a part of the field that was managed by the farmer as usual (i.e. not the zero plots). Each proximal sensor measurement was the average of four recordings obtained in four directions, together representing an area of approximately 3 m × 3 m. The Yara N-Sensor is a sensor that records reflectance data in 45 bands 10 nm wide in the 400–900 nm region of the electromagnetic spectrum. Conversion to N-uptake is made through a built-in calibration function developed by Yara (Reusch 2003) and used by the Swedish Board of Agriculture in its monitoring programme. The selected farms cover the main winter wheat districts in Sweden (Fig. 1). Fourteen of the most commonly grown winter wheat cultivars in Sweden were included, seven from Lantmännen SW seed (Malmö, Sweden): 'Brons', 'Festival', 'Hereford', 'Julius', 'Linus', 'Norin', and 'Stava'; and seven from Scandinavian Seed (Lidköping, Sweden): 'Elvis', 'Frontal', 'Mariboss', 'Olivin', 'Praktik', 'RGT Reform' and 'Torp'.

## Tractor-borne proximal sensing

Data on N-uptake were also gathered by tractor scanning in 13 fields (ranging in size from 2 to 30 ha) in the area around the village of Ardala (see Fig. 1) on 27–29 May 2017. A passive Yara N-Sensor® was used and the tractor was driven in a regular pattern over the fields on tramlines at 24 m spacing, recording N-uptake every second (with approximately 3 m between recordings). The N-uptake values from the sensor were

interpolated by ordinary block kriging (Burrough and McDonnell 1989) to the same 20 m × 20 m grid cell size as the Sentinel-2 data, to enable comparisons.

## Satellite remote sensing

The Sentinel-2 satellites (2A and 2B) carry optical instrument payloads that sample 13 spectral bands with different spatial resolution: 10 m (2 [nominal blue], 3 [green], 4 [red] and 8 [broad-band NIR]); 20 m (5, 6, 7 [red-edge], 8A [narrow-band NIR], and 11, 12 [SWIR]); and 60 m (1 [coastal blue], 9 [NIR water vapour], and 10 [SWIR cirrus]) (ESA 2020). Details are given in Table 1.

Sentinel-2 data (both L1C and L2A) were downloaded from the Copernicus Open Access Hub (https://scihub.copernicus.eu/; ESA, EU, download period: 2018–2020). Sentinel-2 products were projected in WGS1984 UTM zone 33 N and organised by tiles following the military grid reference system (MGRS). After downloading, products were visually inspected for haze and clouds. Images that appeared cloud-free on field data points were paired (if within ± 3 days of acquisition) with the handheld proximal sensor data, and Sentinel-2 reflectance values were extracted (using nearest neighbour) from the pixel in which the field measurement was carried out. A total of 251 unique records had both handheld proximal data and remote sensing data. Some field measurements appeared to contain georeferencing errors (the points were outside the field) and were removed. The final dataset contained 242 records after exclusion of such records. Correlation of data from the L1C and L2A products was evaluated for four of the Sentinel-2 bands (3, 4, 6 and 8).

**Table 1** Sentinel-2 satellite data bands with associated spatial resolution, central wavelength (λ) and bandwidth (Width) for sensor A (S2A) and sensor B (S2B) (ESA 2020)

| Band | Spatial resolution | S2A | | S2B | |
|---|---|---|---|---|---|
| | (m) | λ (nm) | Width (nm) | λ (nm) | Width (nm) |
| Band 1—Coastal aerosol | 60 | 443.9 | 27 | 442.3 | 45 |
| Band 2—Blue | 10 | 496.6 | 98 | 492.1 | 98 |
| Band 3—Green | 10 | 560.0 | 45 | 559.0 | 46 |
| Band 4—Red | 10 | 664.5 | 38 | 665.0 | 39 |
| Band 5—Vegetation red edge | 20 | 703.9 | 19 | 703.8 | 20 |
| Band 6—Vegetation red edge | 20 | 740.2 | 18 | 739.1 | 18 |
| Band 7—Vegetation red edge | 20 | 782.5 | 28 | 779.7 | 28 |
| Band 8—NIR | 10 | 835.1 | 145 | 833.0 | 133 |
| Band 8A—Narrow NIR | 20 | 864.8 | 33 | 864.0 | 32 |
| Band 9—Water vapour | 60 | 945.0 | 26 | 943.2 | 27 |
| Band 10—SWIR—Cirrus | 60 | 1373.5 | 75 | 1376.9 | 76 |
| Band 11—SWIR | 20 | 1613.7 | 143 | 1610.4 | 141 |
| Band 12—SWIR | 10 | 2202.4 | 242 | 2185.7 | 238 |

Abbreviations in band descriptions are Near infrared (NIR) and shortwave infrared (SWIR)

## Vegetation indices

To explore how different types of vegetation indices functioned in modelling, five different vegetation indices all based on bands within the spectral region of the proximal sensor were tested for this study. The vegetation indices were calculated from the Sentinel-2 data and were: normalised difference vegetation index (NDVI; Rouse et al. 1974); normalised difference red-edge vegetation index for two different band combinations, bands 8 and 5 (NDRE85), and bands 8 and 6 (NDRE86) (Barnes et al. 2000); modified soil-adjusted vegetation index (MSAVI2; Qi et al. 1994); and leaf chlorophyll index (CI; Gitelson et al. 2003). Two of these indices (NDVI and MSAVI2) are NIR-/red-based and both are already used in CropSAT (Söderström et al. 2017). The other three indices (NDRE85, NDRE86 and CI) use a red/red-edge band combination. Bands in the red-edge region have been shown to be useful in studies of N-uptake (Reusch 2003, 2005). Equations 1–5 show how the indices were calculated, where ρ is reflectance and the subscript indicates the Sentinel-2 band number:

$$NDVI = \frac{\rho_8 - \rho_4}{\rho_8 + \rho_4} \tag{1}$$

$$MSAVI2 = \frac{1}{2}\left[\left(2 \times \rho_8 + 1\right)\sqrt{\left[\left(2 \times \rho_8 + 1\right)^2 - 8 \times \left(\rho_8 - \rho_4\right)\right]}\right] \tag{2}$$

$$NDRE85 = \frac{\rho_8 - \rho_5}{\rho_8 + \rho_5} \tag{3}$$

$$NDRE86 = \frac{\rho_8 - \rho_6}{\rho_8 + \rho_6} \tag{4}$$

$$C = CI_{red-edge} = \left(\frac{\rho_7}{\rho_6}\right) - 1 \tag{5}$$

## Modelling and validation

An overview of the data processing and analyses performed in the study is given in Fig. 2. Regression models for prediction of N-uptake were parameterised between the handheld proximal sensing N-uptake data and the vegetation indices derived from the Sentinel-2 data. To assess the prediction accuracy when applying the model to new sites and dates, a spatiotemporal cross-validation was designed and employed. This method of leave-one-out cross-validation is a model validation technique in which the records are repeatedly split into 'test data' (the record for which a prediction is made) and 'training data' (the records used to parameterise the model). With each iteration, one record was assigned to the test set and the remaining records were assigned to the training set. In order to validate the model in a manner which resembled a practical application in a DSS, any records from the same site as the test record and data collected later in the

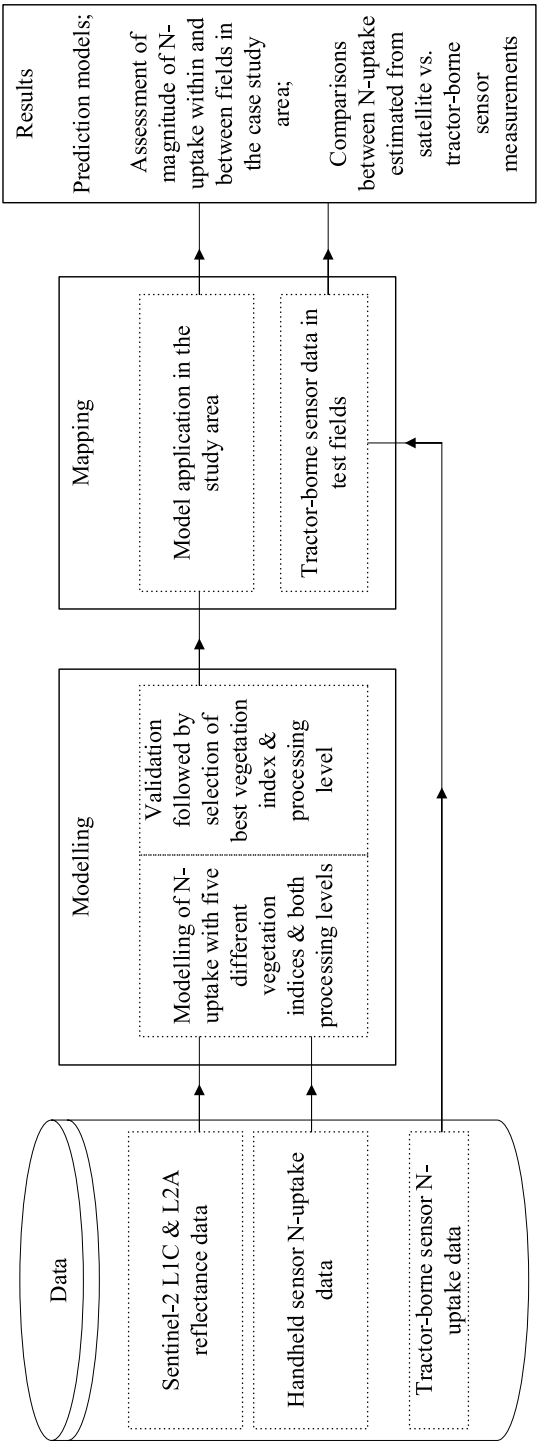


**Fig. 2** Schematic overview of the study. Data are in top of atmosphere (L1C) and bottom of atmosphere (L2A) processing level

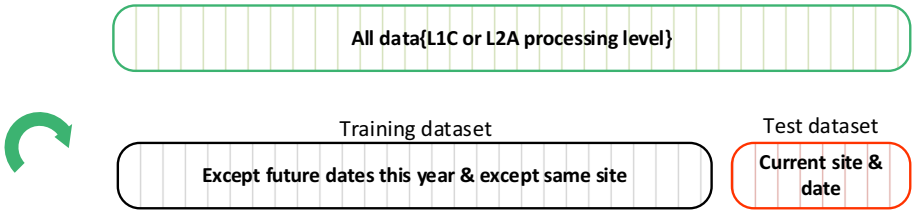


**Fig. 3** Graphical display of the spatiotemporal leave-one-out cross-validation procedure used for regression predictions. A set of all data of either top of atmosphere (L1C) or bottom of atmosphere (L2A) processing level enters the procedure. For each record in the dataset, a model was trained leaving out that record and also leaving out other records from the same site and all records from later dates in the same year. The training set was used to calibrate prediction models and nitrogen (N)-uptake was predicted for the test record

same year (than the date of the test record) were also removed from the training dataset. This was repeated until all 242 records had been tested (Fig. 3).

To determine prediction accuracy, validation measures were calculated from the measured and predicted N-uptake values. The Nash–Sutcliffe modelling efficiency (E) can theoretically take values between $-\infty$ and 1, where an E value of 0 means that the model is just as accurate as a mean of the measured data and an E value of 1 is a perfect fit, which means that the predicted values are equal to the measured values (Nash and Sutcliffe 1970). The mean error (ME) is a measure of the overall prediction bias. The mean absolute error (MAE) is the average of the absolute prediction error. The coefficient of determination ($r^2$) explains the goodness-of-fit of the prediction.

To exemplify possible use of modelling results and to quantify the magnitude of within- and between-field variation in N-uptake, the best fitting prediction model was applied to predict N-uptake within a case study area (Fig. 1), covering 7045 $km^2$ with a high density of winter wheat fields (as determined by winter wheat fields reported in the EU agricultural subsidies system; Swedish Board of Agriculture 2019b). For this, cloud- and haze-free satellite data from 27 May 2017 were used (corresponding to approximately winter wheat growth stage DC37 in this area according to an online service by the Swedish Board of Agriculture; https://etjanst.sjv.se/). Modelled data were extracted for each field (which was reduced in size using a buffer of 15 m along field boundaries to avoid mixed pixel effects) and the magnitude of within-field variation in N-uptake was calculated for the inter-percentile range 2.5–97.5% (to exclude other potential outlier effects).

The satellite-based model predictions of N-uptake were compared with maps resulting from interpolation of the tractor-borne N-sensor measurements. This comparison consisted of two parts: (1) a visual comparison of spatial variation patterns and (2) field-wise correlation analyses between satellite-based and tractor-based values ($r^2$ and MAE).

## Software

To determine which MGRS files matched the field measurement coordinates, the Python programming language was used (Python software foundation, Wilmington, Delaware, USA). Data were stored in a SQLserver database (Microsoft, Redmond, Washington, USA) and analyses were performed using the R programming language (R core team 2018). ArcGIS 10.7 (Esri Inc., Redlands, California, USA) was used for data analysis and display.

## Results

### Data exploration

The data from the L1C and L2A processing levels were found to be linearly correlated to each other in bands, 3, 4, 6 and 8 (Fig. 4). In bands 3 and 4, the L1C values were larger than the L2A values. In bands 6 and 8, the opposite pattern could be seen, where L2A values were smaller than L1C values. In all cases, Pearson correlation coefficient was higher than 98%, with the lowest correlation for band 3. Reflectance values in the individual bands for the two different processing levels were thus very similar in this dataset.

The vegetation indices studied correlated differently with N-uptake measured by the handheld proximal canopy reflectance sensor for both the L1C and L2A processing level datasets (Fig. 5). NDVI and the two different NDRE indices showed weak correlations, with $r^2 < 0.44$ for both L1C and L2A data. As can be seen from the diagram, the CI values were better correlated to the proximal sensor measurements (L1C: $r^2 = 0.78$; L2A: $r^2 = 0.76$). The MSAVI2 values were non-linearly correlated with the field data (L1C: $r^2 = 0.55$; L2A: $r^2 = 0.50$).

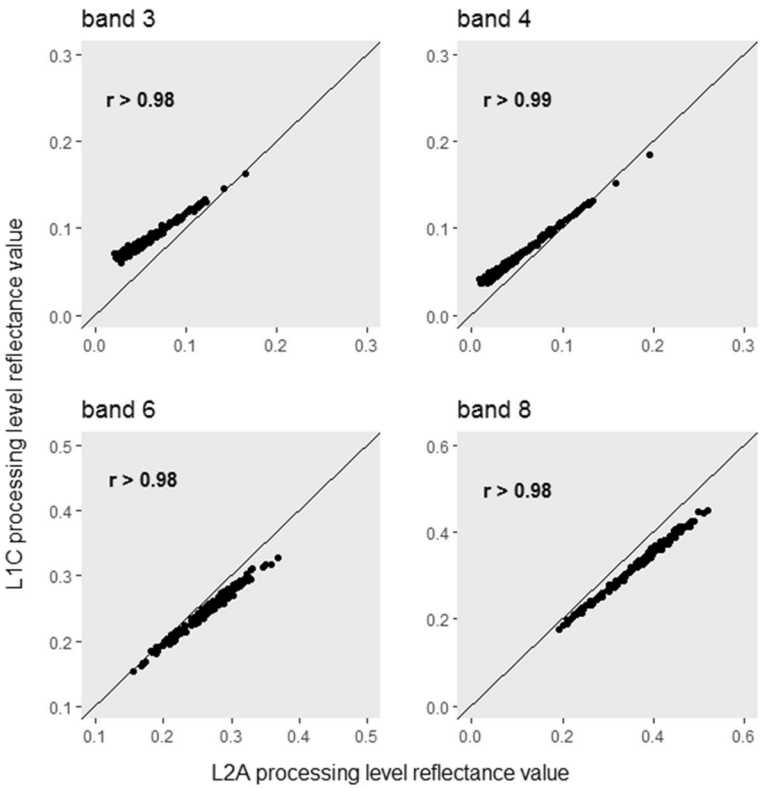


**Fig. 4** Comparison of reflectance values in top of atmosphere (L1C) versus bottom of atmosphere (L2A) processing level products for bands 3, 4, 6 and 8

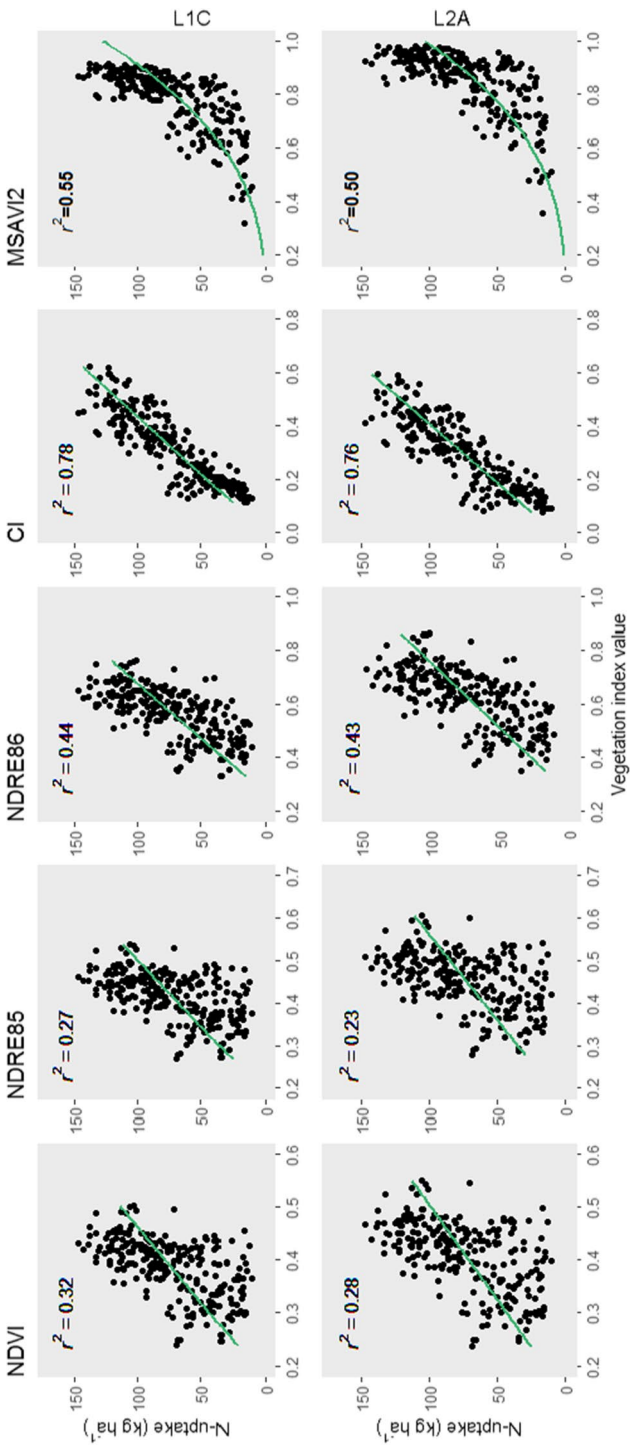


**Fig. 5** Measured nitrogen (N)-uptake plotted against the five different vegetation indices tested for all 14 winter wheat cultivars in growth stages DC22-53 (Zadok et al. 1974). The horizontal axis are vegetation index values, on the vertical axis shows N-uptake (kg ha$^{-1}$) from the ground measurements made with a proximal canopy reflectance sensor, for the two different processing levels top of atmosphere (L1C) and bottom of atmosphere (L2A). A linear model fitted the indices: normalised difference vegetation index (NDVI), normalised difference red-edge index based on band 8 and band 5 (NDRE85), normalised difference red-edge index based on band 8 and band 6 (NDRE86) and chlorophyll index (CI). A non-linear power function fitted the modified soil adjusted vegetation index (MSAVI2)

## N-uptake prediction

The results of the spatiotemporal cross-validation procedure for the different models are summarised in Table 2. Use of L2A data instead of L1C data resulted in only minimal differences in the correlation statistics and modelling was therefore done only with the L1C satellite data. There was a relatively strong linear relationship ($r^2 = 0.74$) between the predicted and observed values. The Nash–Sutcliffe efficiency index confirmed relatively good model performance (E = 0.72). The MAE was 14 kg N ha$^{-1}$ and ME was 4 kg N ha$^{-1}$, reflecting the spread around the 1:1 line in Fig. 6, and the prediction bias was small.

## Model application

The prediction model based on the CI values was applied at around development stage DC37 to all winter wheat fields in the case study area (see Fig. 1). As the indicator maps in Fig. 7 show, fields with high or low within-field variation were spread across the area, but some spatial trends were distinguishable. For example, in the intense cultivation area in the west (the circles to the west in Fig. 7a, c), there was a tendency for fields to have relatively low within-field variability, whereas in the eastern part of the case study area fields with higher within-field variability in N-uptake were common. Of all fields larger than 5 ha, 62% showed variation in N-uptake greater than 30 kg N ha$^{-1}$. The within-field variation in N-uptake (inter-percentile range 2.5–97.5%) in the 4169 different fields ranged between 0 and 105 kg ha$^{-1}$ (summarised in Fig. 8). Less than 50% of the fields were between 5 and 10 ha in size and these had the smallest within-field variation, on average 30 kg N ha$^{-1}$. The magnitude of within-field variation increased with field size, up to 41 kg N ha$^{-1}$ for fields > 30 ha. The histograms in Fig. 8 show this variation, which shows a normal distribution. Field mean values of N-uptake, as measured with the Yara N-sensor, ranged between 28 and 149 kg N ha$^{-1}$, with an average of 90 kg N ha$^{-1}$ (Fig. 9).

Comparisons between N-uptake predicted by the satellite model and the tractor-borne N-sensor are shown in Figs. 10 and 11; Table 3. The $r^2$ values ranged from 0.29 to 0.85 for the 13 fields. When all fields were considered together, $r^2$ was 0.81 and MAE was

**Table 2** Validation statistics (modelling efficiency (E), mean error (ME), mean absolute error (MAE), coefficient of determination ($r^2$)) for prediction models for different vegetation-based indices at two different processing levels, top of atmosphere (L1C) and bottom of atmosphere (L2A)

| | NDVI | NDRE85 | NDRE86 | CI | MSAVI2 |
|---|---|---|---|---|---|
| L1C | | | | | |
| E | 0.30 | 0.16 | 0.41 | 0.72 | 0.46 |
| MAE (kg ha$^{-1}$) | 23 | 25 | 21 | 14 | 20 |
| ME (kg ha$^{-1}$) | 2 | − 1 | 2 | 4 | 8 |
| $r^2$ | 0.31 | 0.20 | 0.42 | 0.74 | 0.55 |
| L2A | | | | | |
| E | 0.15 | 0.08 | 0.41 | 0.70 | 0.36 |
| MAE (kg ha$^{-1}$) | 25 | 26 | 21 | 15 | 22 |
| ME (kg ha$^{-1}$) | − 4 | − 4 | 1 | 5 | 9 |
| $r^2$ | 0.21 | 0.15 | 0.41 | 0.73 | 0.48 |

Normalised difference vegetation index (NDVI); normalised difference red-edge index (NDRE85) based on band 8 and band 5; normalised difference red-edge index (NDRE86) based on band 8 and band 6; chlorophyll index (CI) and modified soil adjusted vegetation index (MSAVI2)

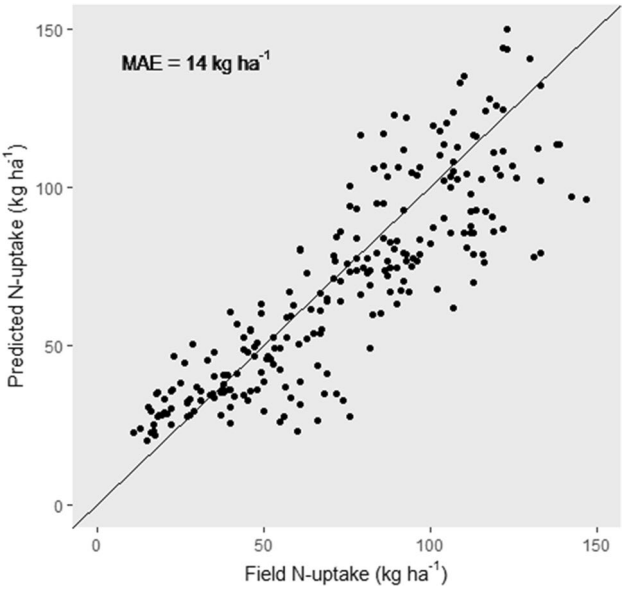


**Fig. 6** Spatiotemporal cross-validation prediction based on a chlorophyll index (CI) model for top of atmosphere (L1C) satellite data versus field nitrogen (N)-uptake obtained from the proximal canopy reflectance sensor. The mean absolute error (MAE) is also shown

7 kg N $ha^{-1}$. High $r^2$ values were more common when the within-field variation was larger. The MAE varied slightly (4–12 kg N $ha^{-1}$) between the fields, and this variation did not appear to be clearly related to field size. Visual comparison revealed that the spatial pattern of within-field variability was fairly similar between maps produced by data from the tractor-borne N-sensor and maps generated from the Sentinel-2 L1C CI-based prediction model. A close-up view of a few fields is shown in Fig. 11.

## Discussion

Using handheld proximal crop sensing data to build the model, it was possible to develop a well-performing, simple linear prediction model for N-uptake from Sentinel-2 data ($r^2 = 0.74$ for the CI-based model with L1C data). Prediction of N-uptake by sensors is done in reality through its correlation with total canopy chlorophyll content, which in turn is closely correlated with total canopy N content (e.g. Schlemmer et al. 2013). Using N-uptake models based on satellite data is a low-cost method to derive decision support for building N fertilisation strategies, quickly and inexpensively, for large cropping areas. In this case, the N-uptake prediction model was general, and 14 different winter wheat varieties were included. In addition, a relatively long period of crop development (DC22-53) was covered. Earlier work by Wolters et al. (2019) and Söderström et al. (2017) showed that satellite-based N-uptake models could be slightly improved if they were cultivar-specific, but this was not done in the present study.

Estimation of N-uptake by means of reflectance data from optical satellite data brings common challenges that arise when using remote sensing data. Irregular product quality


**Fig. 7** Spatial representation of within-field variation in nitrogen (N)-uptake in the case study area (for location, see Fig. 1). One point represents one winter wheat field > 5 ha. The red circles to the left (west) and right (east) highlight areas with visible differences in the magnitude of within-field variation in N-uptake (kg ha$^{-1}$). Background: Sentinel-2 true colour composite with sensing date 27 May 2017

due to interference by clouds and cloud shadows can present difficulties in model calibration or model implementation in a DSS. Satellite data suppliers, in this case ESA, devote much effort to providing high-quality satellite data and are continually striving to improve their available products. However, regardless of ongoing development, some issues like persistent periods of cloud cover are difficult to overcome. Before implementation in a DSS, visual assessment of satellite data quality may be required by DSS providers and users.

With regard to development of models in the present study, there were enough cloud-free images available to get good estimates of N-uptake throughout the season

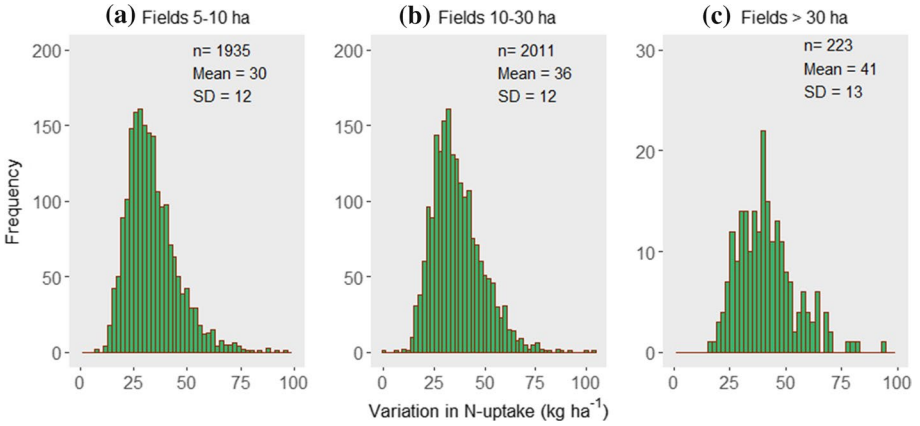


**Fig. 8** Range of variation (inter-percentile range 2.5–97.5%) of nitrogen (N)-uptake within fields (kg $ha^{-1}$) for field sizes **a** between 5 and 10 ha, **b** between 10 and 30 ha and **c** more than 30 ha in the case study area

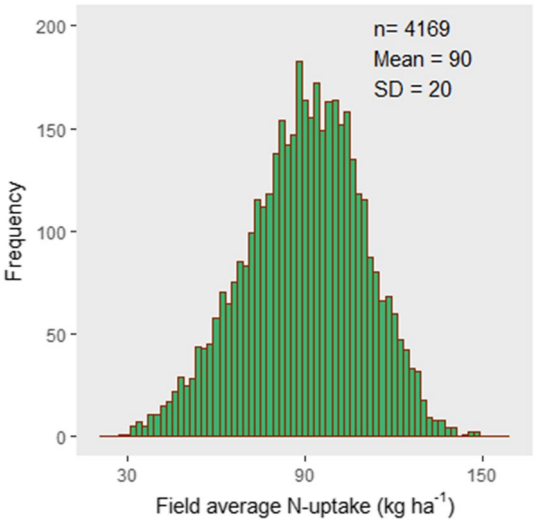


**Fig. 9** Average nitrogen (N)-uptake (kg $ha^{-1}$) in fields > 5 ha in the case study area

of supplementary N fertilisation at the field data locations. The very small differences between models based on the L1C and L2A data (Fig. 5) suggest that the visual inspection of quality of the L1C images performed during the selection process was sufficient to yield directly usable data. L1C products gave slightly lower index values for the MSAVI2 vegetation index than the L2A products (Fig. 5). This was due to somewhat higher reflectance values in band 4 and lower reflectance values in band 8 (in L1C compared with L2A).

It was shown that, using a Sentinel-2 prediction model of N-uptake, it was possible to map the range of within-field variation over large areas. This can be valuable information for farmers, advisory workers and precision agriculture retailers, and in environmental protection-based programmes such as the Swedish 'Focus on Nutrients' Initiative (OECD 2018). In highly variable fields, the potential benefit of precision agriculture practices is likely to be greater from both an economic and an environmental point of view. Many fields in this study (> 62%) showed within-field variation exceeding 30 kg N $ha^{-1}$. The

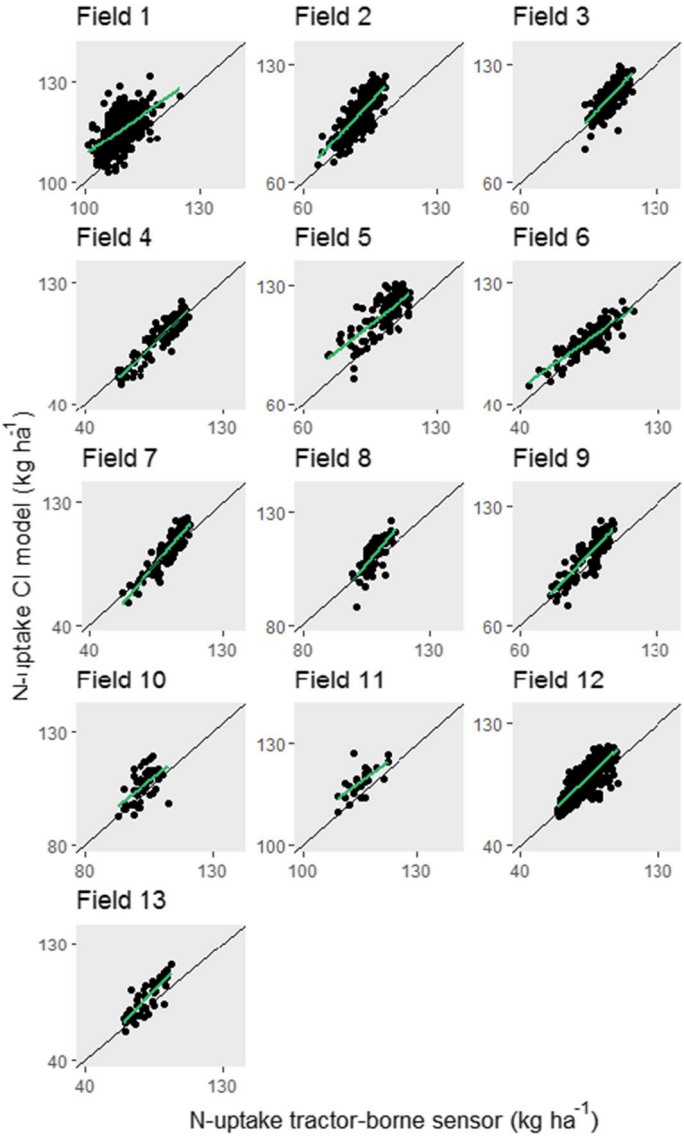


**Fig. 10** Nitrogen (N)-uptake from the tractor-borne sensor compared with satellite-based prediction model N-uptake for the Ardala fields (see also Table 3; Fig. 11)

data presented therefore support previous conclusions by e.g. the European Union (EEA 2019; EPRS 2016) that VRA of N fertilisers is the way forward in using resources more efficiently and thereby also potentially mitigating emissions of greenhouse gases.

A future application of N-uptake prediction models is as part of N fertilisation algorithms, with the aim of deriving an economically optimum N-rate. For other crops and small fields that require high spatial detail, prediction models based on instruments mounted on other vehicles or stationary systems may be applicable. Having more

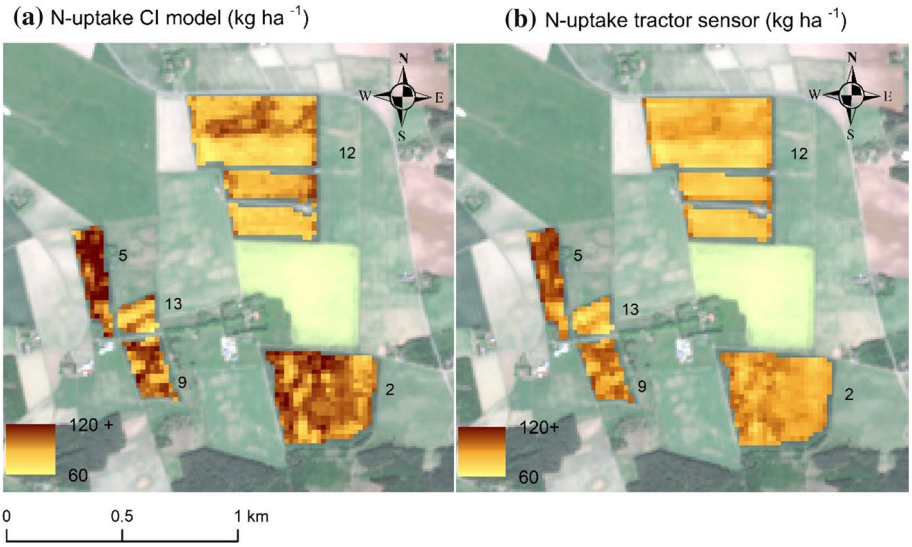


**Fig. 11** Close-up view of some of the Ardala fields (location in Fig. 1). Left: the nitrogen (N)-uptake calculated from the satellite prediction model. Right: Interpolated N-uptake data from the tractor-borne N-sensor within two days of the aquisition date of the satellite image. The different fields are labelled with their field identification (ID) number (cf. Table 3; Fig. 10). Background: Sentinel-2 true colour composite with sensing date 27 May, 2017

**Table 3** Comparison of nitrogen (N)-uptake (kg $ha^{-1}$) values produced by tractor-borne Yara N-sensor measurements (N-sensor) with N-uptake maps predicted by a model based on satellite data (Satellite) for 13 fields around Ardala village, arranged by field size (large to small)

| ID no | Field size (ha) | N-sensor (kg $ha^{-1}$) | | Satellite (kg $ha^{-1}$) | | $r^2$ | MAE (kg $ha^{-1}$) |
|---|---|---|---|---|---|---|---|
| | | Min | Max | Min | Max | | |
| 12 | 30.4 | 64 | 103 | 61 | 113 | 0.64 | 7 |
| 1 | 20.7 | 101 | 125 | 103 | 132 | 0.29 | 7 |
| 2 | 17.2 | 68 | 103 | 71 | 124 | 0.65 | 12 |
| 3 | 11.7 | 93 | 118 | 80 | 130 | 0.52 | 6 |
| 4 | 9.2 | 62 | 108 | 54 | 116 | 0.85 | 4 |
| 7 | 6.5 | 62 | 108 | 57 | 119 | 0.85 | 5 |
| 5 | 5.9 | 73 | 116 | 75 | 131 | 0.57 | 11 |
| 6 | 5.6 | 45 | 113 | 54 | 116 | 0.77 | 6 |
| 9 | 5.0 | 75 | 108 | 71 | 121 | 0.71 | 8 |
| 8 | 4.8 | 99 | 116 | 88 | 126 | 0.56 | 5 |
| 10 | 4.2 | 93 | 113 | 93 | 120 | 0.32 | 5 |
| 13 | 3.0 | 65 | 97 | 62 | 114 | 0.70 | 8 |
| 11 | 1.7 | 109 | 122 | 110 | 127 | 0.47 | 4 |
| All | 125.9 | 45 | 125 | 54 | 132 | 0.81 | 7 |

Coefficient of determination ($r^2$) and mean absolute error (MAE) are also shown

reflectance data available from different platforms, for example drones, could help increase model performance via downscaling of algorithms.

Models for N-uptake should ideally be continuously updated to include new cultivars and varying growing conditions. Weekly scanning of crops with proximal sensors over several seasons (as done by the Swedish Board of Agriculture for their advisory programme) provides an invaluable dataset of observations that are useful for producing models that are applicable in seasons with different growing conditions.

Winter wheat is an important staple crop and is widely cultivated in northern Europe (often in large fields), so there is great potential for using modelling techniques based on Sentinel-2 data for this crop. Considering the good resemblance between N-uptake maps from the model based on satellite sensing and those from the commonly used tractor N-sensor (Table 3), it can be inferred that satellite data may also be useful in practical VRA applications.

## Conclusions

It was possible to scale proximal canopy reflectance sensor data to full spatial coverage in wheat production areas in Sweden using Sentinel-2 satellite data. A linear model based on the CI showed the best N-uptake prediction performance for new sites and dates (L1C data: $r^2 = 0.74$ and MAE = 14 kg ha$^{-1}$). Model predictions were not improved when using BOA reflectance values from Sentinel-2 L2A data compared with L1C data.

When Sentinel-2 satellite-based maps of N-uptake were compared with maps based on data from a tractor-borne sensor in 13 fields, a correlation of $r^2 = 0.81$ and MAE = 7 kg N ha$^{-1}$ was found. Visual comparison of the maps showed a similar pattern of spatial variation. It was concluded that the satellite-based model, using CI values from L1C Sentinel-2 data for N-uptake prediction, gave results comparable to a tractor-borne in-field reflectance instrument.

Satellite-based scaling of proximal N-uptake measurements is useful for general assessments of within and between-field variation, making it possible to pinpoint fields where VRA of N would be most useful. The within-field variation in N-uptake exceeded 30 kg N ha$^{-1}$ in 62% of all fields larger than 5 ha, indicating potential for major economic and environmental benefits from within-field VRA.

**Acknowledgements** Thanks to the project "Focus on Nutrients" at the Swedish Board of Agriculture for the georeferenced data on nitrogen uptake obtained by handheld sensor measurements. Thanks also to farmer Henrik Stadig for giving us access to the tractor-scanning data.

**Author contributions** Conceptualisation and method: WS, SM and PK; data collection and preparation: WS and SM; data analysis: WS; first draft preparation: WS; review and editing: WS, SM, PK, RH and SM; All authors have read and agreed to the published version of the manuscript.

**Funding** Open Access funding provided by Swedish University of Agricultural Sciences. This project was funded by Västra Götalandsregionen and the Swedish University of Agricultural Sciences (contract: RUN 2018-00141) together with Dataväxt AB, Sweden.

**Data availability** Data are not openly available, but raw data are accessible: Sentinel-2 data from the European Space Agency (https://scihub.copernicus.eu/dhus/), and compilations of the nitrogen uptake (kg ha$^{-1}$) measurements in newsletters (in Swedish) from the Swedish Board of Agriculture (https://greppa.nu/varatjanster/sasongsnytt.html).

**Code availability** Programming code is not openly available.

## Compliance with ethical standards

**Conflict of interest** The authors declare no conflicts of interest. The funders had no role in the research design; in the collection, analyses, or interpretation of data; in the writing of the manuscript or in the decision to publish the results.



## References

Barnes, E. M., Clarke, T. R., Richards, S. E., Colaizzi, P. D., Haberland, J., Kostrzewski, M., et al. (2000). Coincident detection of crop water stress, nitrogen status and canopy density using ground based multispectral data. In P. C. Robert, R. H. Rust, & W. E. Larson (Eds.), *Proceedings of the 5th international conference on precision agriculture* (pp. 16–19). Madison: American Society of Agronomy.

Basnet, B., Apan, A., Kelly, K., Strong, W., & Butler, B. (2003). Relating satellite imagery with grain protein content. In *Proceedings of the spatial sciences conference* (pp. 22–27). Los Angeles: Spatial Sciences Institute.

Berger, K., Verrelst, J., Féret, J., Wang, Z., Wocher, M., Strathmann, M., et al. (2020). Crop nitrogen monitoring: Recent progress and principal developments in the context of imaging spectroscopy missions. *Remote Sensing of Environment, 242*, 111758.

Börjesson, T., Wolters, S., & Söderström, M. (2019). Satellite-based modelling of protein content in winter wheat and malting barley. In J. Stafford (Ed.), *Precision agriculture, Proceedings of the 12th European conference on precision agriculture* (pp. 581–587). Wageningen: Wageningen Academic Publishers.

Burrough, P. A., & McDonnell, R. A. (1989). *Principles of geographical information systems*. New York: Oxford University Press.

Curran, P. J. (1989). Remote sensing of foliar chemistry. *Remote Sensing of Environment, 30*, 271–278.

Delin, S., & Stenberg, M. (2014). Effect of nitrogen fertilization on nitrate leaching in relation to grain yield response on loamy sand in Sweden. *European Journal of Agronomy, 52*, 291–296.

Drusch, M., et al. (2012). Sentinel-2: ESA's optical high-resolution mission for GMES operational services. *Remote Sensing of Environment, 120*, 25–36.

European Environment Agency (EEA). (2019). *Climate change adaptation in the agriculture sector in Europe*, Report: 04/2019, ISSN 1977-8449.

European Parliamentary Research Service (EPRS). (2016). *Precision agriculture and the future of farming in Europe, Brussels, European parliament*, ISBN 978-92-846-0475-3.

European Space Agency (ESA). (2020). *Copernicus open access hub*. Retrieved February 22, 2020 from https://www.sentinel-hub.com/.

Fletcher, K. (2012). Sentinel-2: ESA's *Optical High-Resolution Mission for GMES Operational Services*, ESA SP-1322/2.

Fredén, C. (1994). *Geology, National Atlas of Sweden*. Stockholm, Sweden: SNA Publishing.

Gascon, F., Bouzinac, C., Thépaut, O., Jung, M., Francesconi, B., Louis, J., et al. (2017). Copernicus sentinel-2A calibration and products validation status. *Remote Sensing, 9*(6), 584.

Gitelson, A. A., Gritz, Y., & Merzlyak, M. N. (2003). Relationships between leaf chlorophyll content and spectral reflectance and algorithms for non-destructive chlorophyll assessment in higher plant leaves. *Journal of Plant Physiology, 160*, 271–282.

Herrmann, I., Karnieli, A., Bonfil, D. J., Cohen, Y., & Alchanatis, V. (2010). SWIR-based spectral indices for assessing nitrogen content in potato fields. *International Journal of Remote Sensing*. https://doi.org/10.1080/01431160903283892.

Kokaly, R. F. (2001). Investigating a physical basis for spectroscopic estimates of leaf nitrogen concentration. *Remote Sensing of Environment, 75*, 153–161.

Main-Knorn, M., Pflug, B., Louis, J., Debaecker, V., Müller-Wilm, U., & Gascon, F. (2017). Sen2Cor for Sentinel-2. In *Conference: Image and signal processing for remote sensing* (3rd ed.). Bellingham: International Society for Optics and Photonics. https://doi.org/10.1117/12.2278218.

Mueller-Wilm, U. (2016). *S2 MPC: Sen2Cor configuration and user manual*, reference: S2-PDGS-MPC-L2A-SUM-V2.3.

Mulla, D. J. (2013). Twenty five years of remote sensing in precision agriculture: Key advances and remaining knowledge gaps. *Biosystems Engineering, 114*(4), 358–371.

Nash, J. E., & Sutcliffe, J. V. (1970). River flow forecasting through conceptual models part I: A discussion of principles. *Journal of Hydrology, 10*(3), 282–290.

Organisation for Economic Co-operation (OECD). (2018). Retrieved February 28, 2020 from https://read.oecd-ilibrary.org/.

Piikki, K., & Söderström, M. (2019). Digital soil mapping of arable land in Sweden, validation of performance at multiple scales. *Geoderma, 352*, 342–350.

Qi, J., Chehbouni, A., Huete, A. R., & Kerr, Y. H. (1994). Modified Soil Adjusted Vegetation Index (MSAVI). *Remote Sensing of Environment, 48*, 119–126.

R Core Team. (2018). *R: A language and environment for statistical computing*. Vienna, Austria: R Foundation for Statistical Computing. Retrieved February 22, 2020 from http://www.R-project.org/.

Reusch, S. (2003). Optimisation of oblique-view remote measurement of crop N-uptake under changing irradiance conditions. In J. Stafford & A. Werner (Eds.), *Precision agriculture. Proceedings of the 4th European conference on precision agriculture* (pp. 573–578). Wageningen: Wageningen Academic Publishers.

Reusch, S. (2005). Optimum waveband selection for determining the nitrogen uptake in winter wheat by active remote sensing. In J. Stafford & A. Werner (Eds.), *Precision agriculture 05* (pp. 261–266). Wageningen: Wageningen Academic Publishers.

Rouse, J. W., Haas, R. H., Scheel, J. A., & Deering, D. W. (1974). Monitoring Vegetation Systems in the Great Plains with ERTS. In *Proceedings, 3rd Earth Resource Technology Satellite (ERTS) Symposium* (1st ed., pp. 48–62).

Sawyer, J. E. (1994). Concepts of variable rate technology with considerations for fertilizer application. *Journal of Production Agriculture, 7*, 195–201. https://doi.org/10.2134/1994.0195.

Schils, R., Olesen, J. E., Kersebaum, K., Rijk, B., Oberforster, M., Kalyada, V., et al. (2018). Cereal yield gaps across Europe. *European Journal of Agronomy, 101*, 109–120. https://doi.org/10.1016/2018.09.003.

Schlemmer, M., Gitelson, A. A., Schepers, J., Ferguson, R., Peng, Y., Shanahan, J., & Rundquist, D. C. (2013). Remote estimation of nitrogen and chlorophyll contents in maize at leaf and canopy levels. *International Journal of Applied Earth Observation and Geoinformation, 25*, 47–54.

Singh, S. P. (2019). Site specific nutrient management through nutrient decision support tools for sustainable crop production and soil health. In *Soil fertility management for sustainable development* (pp. 13–23). Singapore: Springer.

Söderström, M., Börjesson, T., Pettersson, C. G., Nissen, K., & Hagner, O. (2010). Prediction of protein content in malting barley using proximal and remote sensing. *Precision Agriculture, 11*, 587–599.

Söderström, M., Piikki, K., Stenberg, M., Stadig, H., & Martinsson, J. (2017). Predicting nitrogen uptake in winter wheat by combining proximal crop measurements with Sentinel-2 and DMC satellite images in a decision support system for farmers. *Acta Agriculturae Scandinavica, Section B, Soil and Plant Science, 67*, 637–650.

Stafford, J. V. (2000). Implementing precision agriculture in the 21st century. *Journal of Agricultural Engineering Research, 76*(3), 267–275. https://doi.org/10.1006/2000.0577.

Swedish Board of Agriculture. (2019a). *Use of agricultural land 2019, Final statistics*. Retrieved March 18, 2020 from www.Jordbruksverket.se.

Swedish Board of Agriculture. (2019b). *The block map of agricultural land*. Retrieved February 22, 2020 from www.Jordbruksverket.se.

Verrelst, J., Camps-Valls, G., Muñoz-Marí, J., Rivera, J. P., Veroustraete, F., Clevers, J. G. P. W., & Moreno, J. (2015). Optical remote sensing and the retrieval of terrestrial vegetation bio-geophysical properties - A review. *ISPRS Journal of Photogrammetry and Remote Sensing*, *108*, 273–290. https://doi.org/10.1016/j.isprsjprs.2015.05.005.

Wolters, S., Söderström, M., Piikki, K., & Stenberg, M. (2019). Near-real time winter wheat N-uptake from a combination of proximal and remote optical measurements: How to refine Sentinel-2 satellite images for use in a precision agriculture decision support system. In J. Stafford (Ed.), *Precision agriculture,*

*proceedings of the 12th European conference on precision agriculture* (pp. 1001–1007). Wageningen: Wageningen Academic Publishers. https://doi.org/10.3920/978-90-8686-888-9.

Zadok, J. C., Chang, T. T., & Konzak, C. F. (1974). A decimal code for the growth stages of cereals. *Weed Research, 14*, 415–421.

Zhao, C., Liu, L., Wang, J., Huang, W., Song, X., & Li, C. (2005). Predicting grain protein content of winter wheat using remote sensing data based on nitrogen status and water stress. *International Journal of Applied Earth Observation and Geoinformation, 7*, 1–9.